Multi-colony calibration of barium isotopes between shallow-water coral skeletons and in-situ seawater: implications for paleo proxies

Yu-Te Hsieh[a,b,*], Robert Paver[a], Jani T. I. Tanzil[c], Luke Bridgestock[a,d] Jen Nie Lee[e] and Gideon M. Henderson[a]

[a]Department of Earth Sciences, University of Oxford, South Parks Road, Oxford, OX1 3AN, UK

[b]Institute of Oceanography, National Taiwan University, No. 1, Sec. 4, Roosevelt Road, Taipei, 10617, Taiwan

[c]Tropical Marine Science Institute, National University of Singapore, 18 Kent Ridge Road, Singapore, 119227, Singapore

[d]Department of Earth Sciences, University of Cambridge, Downing Street, Cambridge, CB2 3EQ, UK

[e]Faculty of Science and Marine Environment, University of Malaysia Terengganu, 21030 Kuala Nerus, Terengganu, Malaysia

Submitted to *Earth and Planetary Science Letters*

Keywords: barium isotopes; coral; *Porites lutea*; calibration; Singapore Strait; Paleo proxy.

Highlights:

1. This study presents the first multi-colony Ba isotope calibration in *Porites* corals.
2. Seawater seasonal $\delta^{138/134}$Ba variation follows the water-mass mixing in Singapore.
3. Coral skeletons and seawater show an offset of $\Delta^{138/134}Ba_{coral\text{-}sw}$ = -0.28 ± 0.06 ‰.
4. No significant difference in $\Delta^{138/134}Ba_{coral\text{-}sw}$ was found between multiple colonies.
5. Coral skeletal Ba isotopes can be used to trace regional water mass mixing.

***Corresponding author:** yu-te.hsieh@earth.ox.ac.uk; alanhsieh@ntu.edu.tw

Abstract

Barium incorporated in coral skeletons has been widely used as paleo proxies to study terrestrial inputs, upwelling and anthropogenic activities in marine environments. However, these applications often face the challenges of poor replication in the coral skeletal Ba/Ca records from multiple coral colonies and complex Ba sources in coastal environments. Recent studies of Ba isotopes in seawater and deep-sea corals have demonstrated the potential to trace Ba sources and water mixing in the ocean, but there is still a lack of calibrations for Ba isotopes in shallow-water corals. In this study, we present the first multi-colony Ba isotope calibration from three shallow-water *Porites lutea* corals with the contemporaneous in-situ seawater data from the Singapore Strait. We also report the Ba isotope data in the regional water masses around the study area (e.g. South China Sea, Malacca Strait and Johor River estuary). Singapore water Ba concentrations and isotope compositions show a strong influence of terrestrial inputs, following seasonal salinity and monsoon-driven water-mass mixing between the Malacca Strait and the South China Sea. The coral skeletal $\delta^{138/134}$Ba results are generally consistent between the three coral colonies and time-series data closely follow the seasonal $\delta^{138/134}$Ba variations in seawater. Despite the partition coefficient of Ba having a large uncertainty (D_{Ba} = 0.91 ± 0.29), the Ba isotope fractionation between the coral skeletons and seawater is relatively constant ($\Delta^{138/134}Ba_{coral\text{-}sw}$ = -0.28 ± 0.06 ‰) and shows no significant difference between these corals. The mechanism controlling Ba incorporation and isotope fractionation in coral skeletons remains unclear, but the evidence clearly indicates that the coral skeletal Ba is originated from dissolved Ba in seawater. The constant offset of Ba isotopes between coral skeletons and seawater allows for reliable records of seawater $\delta^{138/134}$Ba values. Ba isotopes in

coral skeletons could be used to reconstruct surface water salinity variability in the Singapore Strait, reflecting monsoon driven changes in regional water mass mixing.

1. Introduction

Barium incorporated in coral skeletons (Ba/Ca ratio) has been widely used as paleo proxies in marine environments to indicate freshwater runoff (e.g. McCulloch et al., 2003; Saha et al., 2016; Brenner et al., 2017; Lewis et al., 2018), sediment load (e.g. McCulloch et al., 2003; Fleitmann et al., 2007; Ito et al., 2020) and upwelling (e.g. Lea et al., 1989; Fallon et al., 1999; Reuer et al., 2003; Montaggioni et al., 2006; Walther et al., 2013). These proxies are based on the assumptions that the variation in coral skeletal Ba/Ca ratios is mainly driven by the seawater Ba composition and that the controls of Ba incorporation in coral skeletons are known and correctable. However, several studies have shown that coral Ba/Ca ratios do not always correlate with flooding or upwelling events and show poor reproducibility between multi-colonies (Tudhope et al., 1996; Sinclair, 2005; Lewis et al., 2018; Tanzil et al., 2019). In addition to seawater Ba concentration, culturing experiments and multi-colony calibrations have found that Ba incorporation in coral skeletons can vary with temperature (Dietzel et al., 2004; Gaetani and Cohen, 2006; Gonneea et al., 2017), light (Yamazaki et al., 2021), coral species (LaVigne et al., 2016) and genotypes (Allison et al., 2018).

Barium isotopes in coral skeletons have recently been explored as a new tracer to understand the oceanic Ba cycle, but such applications require the calibration of Ba isotopes between corals and seawater. Hemsing et al. (2018) and Geyman et al. (2019) have established the deep-sea coral Ba isotope calibrations, and their results show constant offsets between the coral skeletal and ambient seawater Ba isotopes. However, calibrations of Ba isotopes between the skeletons of shallow water corals and seawater

are still lacking. Pretet et al. (2016) have shown a wide range of Ba isotope compositions ($\delta^{138/134}$Ba from +0.2 to +1.0 ‰) between different coral species (shallow-water and deep-sea corals) and locations. Liu et al. (2019) report a relatively narrow range of Ba isotope compositions ($\delta^{138/134}$Ba from +0.10 to +0.38 ‰) in a shallow-water coral species *Porites* from several locations in the South China Sea. Neither of these latter studies reported in-situ seawater data, making $\delta^{138/134}$Ba calibrations between shallow-water coral skeletons and seawater ambiguous.

The constant offsets between deep-sea coral skeletons and ambient seawater Ba isotopes demonstrate the potential for using coral skeletons to reconstruct seawater Ba isotope compositions, but also highlight the need for better understanding of the biological and mineralogical controls on the Ba isotope fractionation between coral skeletons and seawater. Although a recent study of inorganic calcite and aragonite precipitation experiments has shown that Ba isotope fractionation in both calcite and aragonite is a function of carbonate precipitation rates (Mavromatis et al., 2020), the isotope fractionation factors are noticeably different between the inorganic precipitation and the measured values in deep-sea corals (Hemsing et al., 2018; Geyman et al., 2019). The assessment of Ba isotope fractionation in shallow-water corals is still limited by the lack of direct calibration between shallow-water corals and in-situ seawater in natural environments.

In this study we present the first multi-colony Ba isotope calibration in three shallow-water *Porites lutea* corals from a turbid reef in Singapore with contemporaneous in-situ seawater data. Two of the coral colonies and seawater samples in this study have been previously studied by Tanzil et al. (2019) to understand the controls of coral skeletal Ba/Ca ratios in this region, which provides a great opportunity for us to apply Ba isotopes as a new tracer to explore the mechanism of Ba incorporation

in coral skeletons. Furthermore, we investigate Ba isotope compositions in the regional water masses (South China Sea and Malacca Strait) and the local river (Johor River estuary, Bridgestock et al., 2021) to understand the seasonal controls of seawater Ba isotopes in the Singapore Strait. This study provides a comprehensive dataset to establish the relationship between the coral skeletal and seawater Ba isotopes, and explores the implications and limitations of using Ba isotopes in coral skeletons as paleo proxies.

2. Samples and methods

2.1. Study area background

Corals and the time-series seawater samples analyzed in this study were collected from the reef of the Kusu Island (KU: 1.22549ºN, 103.74054ºE) (~5 km from the main island of Singapore) in the Singapore Strait (Fig. 1). The Singapore Strait links the Pacific Ocean (South China Sea) and the Indian Ocean (Andaman Sea) through the Malacca Strait. The climate of this region is characterized by a wet NE monsoon season (average rainfall ~300 mm $month^{-1}$) and a relatively dry SW monsoon season (average rainfall ~150 mm $month^{-1}$) (Tanzil et al., 2016). The monsoon-driven currents dominate the seasonal hydrography in this region (Hasan et al., 2012; van Maren and Gerritsen, 2012). During the northeast (NE) monsoon season (November - March), the water pressure gradient from the South China Sea to the Andaman Sea leads a net westward flow from the Singapore Strait to the Malacca Strait. During the southwest (SW) monsoon season (May - September), the reversed wind direction changes the water circulation and derives a net eastward flow from the Malacca Strait to the Singapore Strait. Surface waters in the Malacca Strait feature low salinities (< 31 psu), due to the input of freshwaters from rivers draining the surrounding land mass. Consequently these seasonal changes in water circulation are traced by salinity, with eastward flow

from the Malacca Strait during the SW monsoon resulting in a decrease in the salinity of Singapore Strait surface waters.

The Johor River represents a potentially important local source of freshwater to the Singapore Strait, in addition to the seasonal advection of low salinity water from the Malacca Strait described above. It is located on the southern tip of Malaysia Peninsula and the largest river (annual average discharge of ~80 m^3 s^{-1}) supplying freshwater to the east Johor Strait that connects to the Singapore Strait (Hasan et al., 2012).

2.2. Coral and seawater sampling

Three live massive *Porties lutea* colonies were sampled in April 2016 (KU-K and KU-L) and December 2017 (KU-S-A1) from the Kusu Island (KU). The colonies of KU-K and KU-L were within ~10 m of each other, and KU-S-A1 was about 300 m away from the other two colonies. All three colonies were about 2-3 m below the mid-tide height (tidal range: ~3 m). Samples were cored from the main growth axis of the colony using a pneumatic drill (5 cm diameter and 50 cm long diamond bit core barrel). Sample slices (~7 mm thick) were taken from these cores for the measurements of skeletal luminescence, Ba/Ca and Ba isotopes (Fig. S1).

Time-series seawater samples were collected monthly from the KU site between January 2012 and December 2015. Fourteen seawater samples from 2012 to 2014 and three from 2015 were selected for Ba concentration and isotope measurements in this study to match the periods in which coral subsamples (2012~2014) and the regional water masses (2015~2016) were analyzed. Water samples were filtered with 0.45-micrometer filters and acidified to a pH of 1-2 with distilled HCl before the analyses of Ba concentrations and isotopes. In-situ seawater salinity and temperature (ºC) were monitored monthly from September 2008 to December 2015, using a YSI 6600 multi-

parameter sonde at 1 m below sea surface. The corals (KU-K and KU-L) and seawater samples have been analyzed for long-term monthly-resolution skeletal luminescence and Ba/Ca records by Tanzil et al. (2019). In this study, we selected the coral subsamples from late 2011 to early 2014 with the matching water samples (between February 2012 and January 2014) for Ba concentration and isotope analyses. Discrete water samples collected from the Malacca Strait and the South China Sea between 2015 and 2016 were measured to constrain the Ba compositions in different regional water masses before mixing in the Singapore Strait (Fig. 1). The data and sample locations from previous studies in the Johor River estuary (Bridgestock et al., 2021) and the South China Sea (corals: Liu et al., 2019, and seawater: Cao et al., 2020) are presented for comparison (Fig. 1).

2.3. Coral and seawater Ba/Ca and Ba isotope methods

Ba contamination in coral skeletons has been found to be associated with organic material (Swart et al., 1999). To eliminate this issue, we only selected the coral samples well below the surface tissue layer for this study (Fig. S1). In addition, we also tested the coral cleaning procedure, followed the methods described in Tanzil et al. (2019), to evaluate the impact of organic contamination on the Ba results. In brief, all coral slices were cleaned in a mixture of 1:4 bleach solution (NaOCl, 3-7 % reactive chlorine) and water for 48 hours to decompose organic matter (Nagtegaal et al., 2012), and then sonicated in deionized water (three times, 10 minutes each). As a test of this cleaning procedure, duplicates of certain samples were also subjected to a more rigorous oxidative cleaning method ($NaOCl+HNO_3+H_2O_2$, modified by Shen and Boyle, 1988). Subsamples were milled along the growth axis in each coral slice at every 2-3 mm (~ 30 mg powder, containing ~200 ng of Ba) to achieve a 3-month sample resolution between late 2011 and early 2014.

All the water and coral samples were prepared and analyzed for Ba concentrations and isotopes using the isotope dilution (ID) technique on a thermal ionization mass spectrometer (TIMS) at the University of Oxford, following the methods established by Hsieh and Henderson (2017) and Hemsing et al. (2018). In brief, for seawater samples, 50 mL water (~ 250ng Ba) was weighed and spiked with a ^{137}Ba-^{135}Ba double spike to allow correction for mass fractionation during chemical purification and instrument analysis. Three mL of a 0.9M Na_2CO_3 solution was added to each spiked sample to co-precipitate Ba with $CaCO_3$. The precipitates were centrifuged, cleaned with H_2O and separated from the remaining seawater. For coral samples, cleaned subsample powder was weighed and dissolved in 5 mL 7.5M distilled HNO_3 before adding a ^{137}Ba-^{135}Ba double spike. All the spiked water and coral samples were dried and re-dissolved in 1 mL 3M HCl before purification by cation exchange chromatography (AG50-X8, 200-400 mesh). The overall procedure blank is < 1 ng of Ba (n = 2) for the seawater method and < 0.2 ng of Ba (n = 3) for the coral method.

2.4. Coral chronology

The chronology of the coral cores was based on the seasonal cycles of skeletal luminescence, which has been previously established for the corals collected at the KU site in the Singapore Strait (Tanzil et al., 2016; 2019). The linear relationship between luminescence intensity (green/blue G/B spectral ratio) and seawater salinity was applied to refine the chronology alignment, using AnalySeries 2.0. Although the refined alignment can provide a monthly resolution chronology, the large subsample size for Ba isotope analysis (2-3 mm, ~ 30 mg powder) compromised the resolution to ~3 months. The drilled sample positions between 2013 and 2014 were labelled along the growth axis of each coral slice for references (Fig. S1).

3. Results

In this study, Ba isotopic compositions are reported as the δ-notation $\delta^{138/134}$Ba (‰) relative to the National Institute of Standards and Technology (NIST) 3104a standard:

$$\delta^{138/134}\text{Ba (‰)} = \left(\frac{^{138}\text{Ba}/^{134}\text{Ba}_{\text{sample}}}{^{138}\text{Ba}/^{134}\text{Ba}_{\text{NIST3104a}}} - 1\right) \times 1000 \quad (1)$$

For comparison, data reported in $\delta^{137/134}$Ba in some previous studies have been converted to $\delta^{138/134}$Ba by multiplying by 1.33.

As Ba concentrations are collected by the method of isotope dilution without measuring Ca concentrations, coral Ba concentrations are converted to Ba/Ca (μmol/mol) by assuming a Ca concentration of 40% per mass of the coral (Hemsing et al., 2018). Seawater Ba concentrations are presented in nM. For comparison with coral Ba/Ca ratios, seawater Ba concentrations are normalized by a seawater Ca concentration ([Ca] = 10.3 mM) (Culkin and Cox, 1966). Although the Ca content may vary slightly in coral skeletons (associated with the incorporation of other elements) or seawater (associated with salinity), when compared to the large uncertainty observed between the coral and seawater Ba/Ca ratios (23 ~ 38%, Section 4.2.1), the uncertainty from Ca contents is insignificant.

Some of the Singapore seawater Ba concentrations and coral Ba/Ca ratios have also been previously analyzed by Tanzil et al. (2019) using a quadrupole ICP-MS technique (and laser ablation LA-ICP-MS for coral Ba/Ca). In general, the ICP-MS data correlate with the TIMS results (Fig. S2). However, the ICP-MS water [Ba] data are noticeably lower than the TIMS data, and the LA-ICP-MS coral Ba/Ca data show a much wider range of variation than the TIMS data. Considering that the water $\delta^{138/134}$Ba results show a much better correlation with the TIMS [Ba] data (R^2 = 0.71) than the ICP-MS [Ba] (R^2 = 0.45) and that the coral sample resolutions are different between

225 the TIMS and LA-ICP-MS techniques, we only use the TIMS results for direct
226 comparison and discussion.

227 **3.1. Standard reference material results**

228 Standards and samples generally show an internal precision of $\delta^{138/134}$Ba
229 between 0.01 and 0.02 ‰ (± 2SE, n = 540) during each isotope analysis. The long-term
230 precision and accuracy were monitored with a secondary Ba standard NBS-127 over
231 two years, $\delta^{138/134}$Ba = -0.29 ± 0.02 ‰ (2SD, n = 14), which is in agreement with
232 published values in previous studies ($\delta^{138/134}$Ba = -0.27 ± 0.02 ‰; Horner et al., 2017;
233 and -0.29 ± 0.01 ‰; Crockford et al., 2019). Accuracy is also monitored by processing
234 a coral powder standard JCp-1 alongside samples, $\delta^{138/134}$Ba = +0.29 ± 0.03 ‰ and
235 Ba/Ca = 7.1 ± 0.3 μmol/mol (2SD, n = 4), which agree with published values in
236 previous studies ($\delta^{138/134}$Ba = +0.29 ± 0.03 ‰; Horner et al., 2015; +0.21 ± 0.01 ‰;
237 Pretet et al., 2015; +0.25 ± 0.03 ‰; Hemsing et al., 2018; +0.30 ± 0.03; Liu et al., 2019;
238 +0.28 ± 0.03 ‰; Geyman et al., 2019). In this study, two simulated carbonate standard
239 solutions, NIST RM 8301 Coral and Foram, have been analysed and reported for
240 $\delta^{138/134}$Ba values for the first time (Coral $\delta^{138/134}$Ba = +0.10 ± 0.02 ‰; Foram $\delta^{138/134}$Ba
241 = +0.05 ± 0.02 ‰). Their Ba/Ca ratios (Coral Ba/Ca = 6.1 ± 0.2 μmol/mol; Foram
242 Ba/Ca = 4.0 ± 0.1 μmol/mol) also agree with the inter-laboratory results (Stewart et al.,
243 2020).

244 **3.2. Water results**

245 Singapore surface seawater Ba concentrations and $\delta^{138/134}$Ba values vary from
246 43.0 to 60.2 nM and from +0.32 to +0.49 ‰ respectively in the KU site (Table S1). The
247 seasonal variations correspond to the annual salinity cycles, ranging from 29.3 to 32.1
248 psu between January 2012 and January 2014 (Fig. 2; Section 4.1 and 4.3). During the
249 SW monsoon season (May - September), Singapore seawater Ba concentrations are

generally high (> 53 nM) and the $\delta^{138/134}$Ba values are low (< +0.40 ‰), which coincides with the periods of low salinity (< 31 psu). At the beginning of the NE monsoon season (~November), Singapore seawater shows the lowest [Ba] (< 46 nM) and the highest $\delta^{138/134}$Ba values (> +0.48 ‰), which coincides with the maximum salinity (> 32 psu) of each year.

The surface seawater samples collected from the southern-end of the South China Sea (around the Malaysian east coast) show the lowest [Ba] (< 43 nM), the highest $\delta^{138/134}$Ba value (> +0.5 ‰) and the highest salinity (33 psu) in this study (Table S1). In contrast, water samples collected from the Malacca Strait show relatively high [Ba] (55.0 ~ 71.9 nM), low $\delta^{138/134}$Ba values (+0.30 ~ +0.41 ‰) and low salinity (29 ~ 30 psu) compared to the South China Sea waters. Samples spanning the estuarine mixing zone of the Johor River data from Bridgestock et al. (2021) show high [Ba] (79.2 ~ 837.9 nM), low $\delta^{138/134}$Ba values (+0.34 ~ -0.02 ‰) and lower salinity (0 ~ 27 psu), with an estimated endmember composition of net river inputs of [Ba] = 1039 ± 318 nM and $\delta^{138/134}$Ba = 0.06 ± 0.12 ‰. Seawater samples from the Malacca Strait, South China Sea and Johor River estuary were collected during a different period (2015-2017) to the KU seawater contemporaneous to the sampled coral growth period (2012-2013). However, additional KU seawater samples collected in 2015 show comparable results to those collected in 2012 and 2013 (Table S1).

3.3. Coral skeletal results

Coral skeletal Ba/Ca ratios vary between 3.1 and 6.9 μmol/mol in these three coral colonies (KU-K, KU-L and KU-S-A1) from late 2011 to early 2014 (Table S2), while the Singapore seawater Ba/Ca ratios vary between 4.4 and 6.9 μmol/mol at the KU site over the similar period (Fig. 2). Although the values of coral and seawater Ba/Ca ratios overlap, temporal trends in the coral Ba/Ca ratios are inconsistent between

275 the three colonies. In contrast, coral $\delta^{138/134}$Ba values vary between +0.07 and +0.22 ‰
276 and show a similar temporal trend between each colony (Fig. 2b). The trends of coral
277 $\delta^{138/134}$Ba in all three colonies follow the seawater $\delta^{138/134}$Ba annual cycle reasonably
278 well (see Section 4.2). Direct comparisons for $\delta^{138/134}$Ba and Ba/Ca data between the
279 corals and seawater are summarized in Fig. S3.

280 In the organic cleaning test results, Tanzil et al. (2019) have shown that the
281 cleaning procedures result in no significant difference in coral Ba/Ca ratios between the
282 NaOCl-only method and the NaOCl+HNO_3+H_2O_2 method in these Singapore corals.
283 The set of the samples measured for Ba isotopes in this study shows no detectable
284 difference in $\delta^{138/134}$Ba between the cleaning methods either (NaOCl only: +0.15 ± 0.03
285 ‰; NaOCl+HNO_3+H_2O_2: +0.14 ± 0.03 ‰), which suggests that the coral skeletal Ba
286 signals are unlikely to be the result of organic matter. Geyman et al. (2019) have also
287 found no detectable difference with or without additional oxidizing treatment (H_2O_2)
288 in the deep-sea bamboo coral cleaning experiments. Although organic contamination is
289 not a major issue in this study, assessments of organic Ba isotope compositions can
290 help us to investigate this issue in future studies. Furthermore, organic Ba isotope
291 compositions can improve our understanding of Ba isotope cycling along different Ba
292 incorporation pathways in corals.

293

294 **4. Discussion**

295 **4.1. Regional water mass mixing controls salinity, Ba concentrations and $\delta^{138/134}$Ba**
296 **of Singapore Strait waters**

297 Comparing with the global seawater $\delta^{138/134}$Ba and 1/[Ba] data, Singapore
298 waters are isotopically lighter than other open ocean seawaters at any given Ba
299 concentration (Fig. 3), which reflects the strong influence of terrestrial inputs in this

region. For example, Singapore waters show a maximum offset of $\delta^{138/134}$Ba ~ 0.15 ‰ lower than the global seawater at [Ba] ~ 60 nM (1/[Ba] ~ 0.017 nM^{-1}). Previous studies have shown that the effective riverine inputs, accounting for the desorption of Ba from suspended river sediments in estuaries, contributes isotopically light Ba, featuring $\delta^{138/134}$Ba = -0.01 to +0.11 ‰, to the surface ocean (Hsieh and Henderson, 2017; Bridgestock et al., 2021).

Singapore surface seawater Ba concentrations and isotope compositions closely follow the seasonal sea surface salinity cycle (Fig. 2). The link between Ba contents and salinity in the coastal surface seawater are typically associated with local riverine freshwater inputs (Coffey et al., 1997; Joung and Shiller, 2014) or upwelling (Montaggioni et al., 2006). At a larger scale, relationships between salinity and Ba can trace the mixing of water masses that have received different magnitudes of freshwater inputs, from different riverine sources with distinct Ba concentrations (e.g. Taylor et al., 2003). Sea surface salinity and Ba concentrations show no correlation with the local rainfall in Singapore, suggesting riverine freshwater inputs from local rivers are not the key driver of these relationships (Fig. S4). Furthermore, upwelling is not an important source supplying Ba to the Singapore waters either, given that the Singapore Strait is located on the inner continental Sunda shelf with an average shallow water depth < 30 m (Bird et al., 2006). Instead, the relationships between salinity, Ba concentration and $\delta^{138/134}$Ba likely result from the mixing of surface seawaters that have received different magnitudes of freshwater input at a regional scale.

The $\delta^{138/134}$Ba and 1/[Ba] data in the regional water masses (South China Sea, Malacca Strait and Johor River estuary from this study; Cao et al., 2020; Bridgestock et al., 2021) generally follow the mixing trend through the Singapore water data (Fig. 3). The South China Sea and Malacca Strait waters seasonally circulate through the

325 Singapore Strait, driven by the monsoon currents, and hence play an important role in
326 the Ba and salinity cycles in this region (Tanzil et al., 2019). For instance, during the
327 SW monsoon season (May – September), the eastward current brings the low salinity,
328 high [Ba] and low $\delta^{138/134}$Ba water from the Malacca Strait into the Singapore Strait,
329 although it is usually a dry season in Singapore (Fig. 2a and d).
330 To assess the regional riverine freshwater Ba end-member compositions, the
331 linear regressions through the Singapore seawater [Ba] and salinity data and the
332 $\delta^{138/134}$Ba and 1/[Ba] data show an interception of [Ba] and $\delta^{138/134}$Ba at salinity zero of
333 192 ± 30 nM and 0.08 ± 0.03 ‰ respectively (Fig. 4). These values represent the
334 effective regional freshwater Ba end-member, accounting for the average freshwater
335 input to the Malacca Strait, seasonality and the net effects of estuarine processes (Ba
336 desorption from suspended river sediments) in this region. Although the regional
337 freshwater end-member [Ba] is about 5 times smaller than the value reported for the
338 Johor River (1039 ± 318 nM; Bridgestock et al., 2021), their $\delta^{138/134}$Ba values are not
339 significantly different (Johor end-member $\delta^{138/134}$Ba = 0.06 ± 0.12 ‰) and the mixing
340 trends of $\delta^{138/134}$Ba and 1/[Ba] are not separable between the Johor River and other
341 freshwater inputs in this region (Fig. 5). This implies that the riverine end-member [Ba]
342 values may differ hugely between rivers due to various bedrock Ba contents,
343 weathering processes or rainwater dilution. However, the agreement in end-member
344 $\delta^{138/134}$Ba values may reflect a narrower range of the bedrock Ba isotope compositions
345 in this region and a consistent isotope fractionation associated with the weathering
346 processes.
347 Overall, the correlations between seawater salinity, [Ba] and $\delta^{138/134}$Ba values
348 suggest that seawater [Ba] and $\delta^{138/134}$Ba values may potentially be used as proxies for
349 tracing salinity changes in the Singapore Strait (Fig. 4). The main cause of these salinity

(and hence [Ba] and $\delta^{138/134}$Ba values) variations are changes in the mixing of low salinity Malacca Strait surface waters, with higher salinity South China Sea surface waters, driven by monsoon currents. Thus, the interpretation of salinity and Ba records in Singapore seawater should reflect the climate variability in the Asian monsoon. However, freshwater inputs from local rivers, mainly the Johor River, and rainfall could act as a secondary control on Singapore Strait surface water salinity, [Ba] and $\delta^{138/134}$Ba values. In the following sections, we access the utility of Ba/Ca and $\delta^{138/134}$Ba values of shallow-water corals for reconstructing pass seawater Ba concentrations and $\delta^{138/134}$Ba values, and hence potential past climate variability in the Asian monsoon.

4.2. Barium in coral skeletons

4.2.1. Barium partition coefficient D_{Ba}

Singapore coral skeletal and seawater Ba/Ca ratios generally lie within a similar range, but sometimes the ratios vary widely between the three *Porites lutea* coral colonies and deviate significantly from the seawater values (Fig. 6b). Detailed comparisons of coral skeletal Ba/Ca and environmental conditions in the Singapore coral reefs have been conducted by Tanzil et al. (2019). As for the high turbidity and complex setting in the Singapore water, no simple conclusion has yet been drawn to explain whether the incorporation of Ba in the Singapore coral skeletons is from dissolved or particulate Ba. The new data from this study provide an opportunity to improve our understanding of the incorporation of Ba in coral skeletons by directly comparing the coral skeletal Ba/Ca and $\delta^{138/134}$Ba results.

To understand the controls of Ba incorporation from seawater into coral skeletons, the relationship between the coral skeleton and in-situ seawater Ba/Ca ratios is expressed as the partition coefficient (D_{Ba}):

$$D_{Ba} = (Ba/Ca)_{coral}/(Ba/Ca)_{sw} \quad (2)$$

As the coral sample resolution (~3 months) and the period of the seawater Ba data are not always aligned, the unsampled seawater data are linearly interpolated between the measured data points (Fig. 2a) and a 3-month average seawater Ba/Ca trend (Fig. 6b) was reconstructed using the measured and interpolated data (Table S3). The 3-month average seawater Ba/Ca_{sw} data are used for the D_{Ba} calculation.

The D_{Ba} values range from 0.64 to 1.31 between the three coral colonies in this study (Table S4) with a mean value of D_{Ba} = 0.91 ± 0.29 (2SD, n = 20), which is in reasonable agreement with the reported values for *Porites* in previous studies (e.g. 0.5 ~ 1.5, LaVigne et al., 2016; Allison et al., 2018). Although the mean values of D_{Ba} between the three coral colonies are consistent, the relative uncertainty (± 2RSD 23 ~ 38 %, Table S4) is large and hence unable to precisely distinguish the maximum difference in the Singapore Strait seawater [Ba] (i.e. (the maximum [Ba] – the minimum [Ba])/(the average [Ba]); (60.2 nM – 43.0 nM)/52.8 nM = 33%). Culturing and inorganic experiment studies have both shown that Ba partitioning in aragonite is controlled by temperature, light and the aragonite growth rates (Gaetani and Cohen, 2006; Gonneea et al., 2017; Mavromatis et al., 2018; Yamazaki et al., 2021). However, considering that the three coral colonies in this study were mostly growing under similar environmental conditions (e.g. annual SST: 29.4 ± 0.8 ºC) and that the D_{Ba} values show no correlation with the skeletal linear extension rates (0.99 ~ 1.74 cm/y, Fig. 7c), the variation of D_{Ba} cannot be easily explained by these factors. Apart from the environmental controls, culturing experiments have also shown that coral genotypes may have significant impacts on the variation of D_{Ba} (Allison et al., 2018).

4.2.2. Barium isotope fractionation $\Delta^{138/134}Ba_{coral\text{-}sw}$

399 The coral skeletal $\delta^{138/134}Ba$ values are reasonably consistent between the three
400 coral colonies and follow the seawater $\delta^{138/134}Ba$ seasonal cycle (Fig. 6a). However,
401 there is no correlation between coral $\delta^{138/134}Ba$ values and Ba/Ca ratios (Fig. 7a). To
402 understand the relationship of $\delta^{138/134}Ba$ values between coral skeletons and in-situ
403 seawater during the incorporation of Ba, the offset between the coral skeletal and
404 seawater $\delta^{138/134}Ba$ values is expressed as the isotope fractionation factor ($\Delta^{138/134}Ba_{coral-sw}$):

405

406 $$\Delta^{138/134}Ba_{coral-sw} = \delta^{138/134}Ba_{coral} - \delta^{138/134}Ba_{sw} \quad (3)$$

407 As mentioned above, seawater $\delta^{138/134}Ba_{sw}$ values are also taken from a 3-month
408 average to match the sample resolution between waters and corals. The 3-month
409 average seawater $\delta^{138/134}Ba$ data (Table S3, Fig. 6a) trend was reconstructed using the
410 linearly interpolated $\delta^{138/134}Ba$ data and the measured data points in the Singapore
411 seawater (Fig. 2a).

412 The $\Delta^{138/134}Ba_{coral-sw}$ values (-0.23 to -0.33 ‰) show more consistent results than
413 the D_{Ba} values between the three *Porites* colonies (Table S4). The mean value
414 ($\Delta^{138/134}Ba_{coral-sw}$ = -0.28 ± 0.06 ‰, 2SD, n = 20) is within the range (-0.01 ~ -0.37 ‰)
415 observed in previous studies (Pretet et al., 2016; Hemsing et al., 2018; Geyman et al.,
416 2019; Liu et al., 2019), confirming that coral skeletons preferentially incorporate light
417 Ba isotopes from seawater. For comparisons of the *Porites* results only, a much smaller
418 value ($\Delta^{138/134}Ba_{coral-sw}$ = -0.01 ‰) has been reported by Pretet et al. (2016) from one
419 cultured coral, but this has a relatively large uncertainty (± 0.16 ‰, 2SD). A similar
420 estimate ($\Delta^{138/134}Ba_{coral-sw} \approx$ -0.3 ‰) has been reported by Liu et al. (2019) from natural
421 corals but without the support of ambient seawater data.

422 A recent experimental study has shown that Ba isotope fractionation in
423 inorganic aragonite precipitation is a function of the aragonite growth rate, and the

aragonite Ba isotope fractionation $\Delta^{138/134}Ba_{aragonite\text{-}fluid}$ is correlated with the D_{Ba} values (Mavromatis et al., 2020). However, the $\Delta^{138/134}Ba_{coral\text{-}sw}$ values in the aragonitic corals in this study show no correlation with the D_{Ba} values or the linear extension rates (Fig. 7b and d). Similar observations have also been found in deep-sea corals (Hemsing et al., 2018; Geyman et al., 2019). The inorganic experiment and the transition state theory model have shown that Ba isotope fractionation ($\Delta^{138/134}Ba_{aragnoite\text{-}fluid}$) decreases from +0.33 to -0.13 ‰ when the aragonite growth rate increases from $10^{-8.7}$ to $10^{-7.6}$ mol/m^2/s (Mavromatis et al., 2020). If we apply a typical range of the growth rates for *Porites* ($10^{-5.7}$ to $10^{-5.2}$ mol/m^2/s, Mollica et al., 2018) to the same transition state theory model, coral aragonite should result in an extremely negative isotope fractionation (e.g. $\Delta^{138/134}Ba_{aragnoite\text{-}fluid} \approx$ -2.6 ‰), However, the observed values in aragonitic corals from this study ($\Delta^{138/134}Ba_{coral\text{-}sw}$ = -0.28 ‰) and previous studies (-0.01 ~ -0.3 ‰; Pretet et al., 2016; Hemsing et al., 2018; Liu et al., 2019) are nowhere close to this model prediction. These results imply that growth rates may not be the only control of Ba isotope fractionation in coral skeletons.

Several hypotheses of the Ba incorporation in coral skeletons have been discussed in Tanzil et al. (2019), which mainly involve (1) incorporating dissolved Ba from seawater and (2) ingesting Ba-rich particles. The co-varying $\delta^{138/134}Ba$ values between the coral skeletons and seawater strongly suggest that the skeletal Ba originates from seawater, which is either the dissolved Ba or the Ba particles formed in seawater (e.g. barite). The typical offset in $\delta^{138/134}Ba$ values between marine barite and seawater ($\Delta^{138/134}Ba_{barite\text{-}sw}$) is around -0.5 ‰ (Horner et al., 2017; Bridgestock et al., 2018), which is too large to explain the offset observed in corals ($\Delta^{138/134}Ba_{coral\text{-}sw}$ = -0.28 ‰). Therefore, barite is unlikely to be the major phase in the incorporation of Ba in coral skeletons. Barium may exist as witherite ($BaCO_3$) or associate with organic matter in

449 coral skeletons. However, witherite has a much smaller isotope fractionation factor
450 ($\Delta^{138/134}Ba_{witherite\text{-}fluid}$ ≈ -0.09 ‰, Mavromatis et al., 2016) than the coral value.
451 Regarding the organic matter, as discussed above, the cleaning tests suggest that the
452 skeletal Ba is unlikely to be associated with organic matter (Section 3.3).

453 Although there is no direct evidence to support the presence of $BaCO_3$ in
454 aragonite precipitates or corals, especially when the experiment solution and seawater
455 are undersaturated with respect to $BaCO_3$, the formation of $BaCO_3$ cannot be
456 completely excluded in microenvironments (Mavromatis et al., 2018). Therefore, can a
457 combined effect of (1) $BaCO_3$ precipitation and (2) the exchange reaction (replacing
458 Ca^{2+} with Ba^{2+} in $CaCO_3$) be the main control of Ba incorporation in aragonitic corals?
459 If we assume that a certain fraction of the coral skeletal Ba is incorporated as $BaCO_3$
460 precipitation ($\Delta^{138/134}Ba_{witherite\text{-}fluid}$ ≈ -0.09 ‰) and the rest is through the exchange
461 reaction ($\Delta^{138/134}Ba_{aragnoite\text{-}fluid}$ ≈ -2.6 ‰), to get a combined $\Delta^{138/134}Ba_{coral\text{-}sw}$ of -0.28 ‰
462 in corals, it would require at least 92% of the Ba incorporation to be $BaCO_3$
463 precipitation and only 8% by the exchange reaction. This is unlikely to be the case,
464 given the difficulty to find evidence of $BaCO_3$ in aragonite precipitates and corals.

465 Pretet et al. (2016) have suggested that biological effects may control the
466 variation in $\Delta^{138/134}Ba_{coral\text{-}sw}$ values. In this study, however, the relatively constant
467 $\Delta^{138/134}Ba_{coral\text{-}sw}$ values suggest that no measurable biological effect has been observed
468 between the multiple *Porites* colonies. Similarly, the $\Delta^{138/134}Ba_{coral\text{-}sw}$ values in deep-
469 sea corals are insensitive to different species, locations and depths (Hemsing et al.,
470 2018; Geyman et al., 2019). In fact, aragonitic corals share a similar range of
471 $\Delta^{138/134}Ba_{coral\text{-}sw}$ values (-0.28 ± 0.06 ‰, this study; -0.21 ± 0.08 ‰, Hemsing et al.,
472 2018), regardless of deep-sea or shallow water corals, which cover a wide range of
473 temperature, light and food conditions. In contrast, calcitic corals show a consistently

474 different $\Delta^{138/134}Ba_{coral\text{-}sw}$ value (-0.37 ± 0.03 ‰; Geyman et al., 2019) from aragonitic
475 corals. These results suggest that the mineralogical controls may play a more important
476 role than biological effects in the Ba isotope fractionation in coral skeletons.
477 Although the exact mechanism of coral calcification remains an interesting
478 question, there is growing evidence to support the idea that trace elements, including
479 Ba, are provided from seawater and incorporated into amorphous calcium carbonate
480 (ACC) particles as a precursor phase prior to aragonite precipitation (Mass et al., 2017;
481 Evans et al., 2020). The Ba isotope results of this study also suggest that the coral
482 skeletal Ba is originated from dissolved Ba in seawater. More detailed studies are still
483 required to improve our understanding of the controls of Ba incorporation and isotope
484 fractionation in coral skeletons (e.g. Ba isotopes in ACC and different coral genotypes).
485 Nevertheless, the uncertainty in $\Delta^{138/134}Ba_{coral\text{-}sw}$ between the three *Porites lutea* corals
486 in Singapore is relatively small (±0.06 ‰), compared to the maximum variation of the
487 seawater $\delta^{138/134}Ba$ values seen in the Singapore Strait (i.e. 0.17 ‰; 0.32 vs. 0.49 ‰).
488 In comparison, the difference between the uncertainty in $\Delta^{138/134}Ba_{coral\text{-}sw}$ and seawater
489 $\delta^{138/134}Ba$ is much larger than the difference between the uncertainty in DBa and
490 seawater [Ba] (Section 4.2.1), which implies that the coral skeletons could be used to
491 reconstruct a more reliable history of seawater $\delta^{138/134}Ba$ values than Ba concentrations
492 in the Singapore Strait in the past.
493
494 **4.3. Implications for coral $\delta^{138/134}Ba$ as paleo proxies in the coastal ocean**
495 The coral skeletal $\delta^{138/134}Ba$ and Ba/Ca records may be used as a paired paleo
496 proxy to reconstruct the history of water mixing and local freshwater inputs in the
497 Singapore Strait, as shown in Fig. 3. We applied the partition coefficient (D_{Ba} = 0.91 ±
498 0.29) and isotope fractionation factor ($\Delta^{138/134}Ba_{coral\text{-}sw}$ = -0.28 ± 0.06 ‰) to the coral

499 Ba data to estimate the seawater [Ba] and $\delta^{138/134}$Ba values during 2012 and 2013 in the
500 Singapore Strait. In Fig. 8, the coral reconstructed seawater results show a poor
501 relationship between the $\delta^{138/134}$Ba and 1/[Ba] data ($R^2 = 0.03$), which is due to the large
502 uncertainty in D_{Ba}. This observation highlights the difficulty of using both Ba/Ca and
503 $\delta^{138/134}$Ba values as a paired proxy in the shallow-water corals to reconstruct the history
504 of seawater Ba cycle.

505 Since seawater $\delta^{138/134}$Ba values follow the seasonal sea surface salinity in the
506 Singapore Strait (Fig. 2), can the coral skeletal $\delta^{138/134}$Ba values be used alone as a paleo
507 salinity proxy? This application requires a key assumption that the mixing relationship
508 between $\delta^{138/134}$Ba and salinity stays constant over the time periods of interest.
509 However, this relationship is not only set by the freshwater and seawater end-member
510 $\delta^{138/134}$Ba compositions but also their Ba concentrations, according to the end-member
511 mixing model.

512 In the open ocean, seawater $\delta^{138/134}$Ba and [Ba] compositions are likely to
513 remain constant from decadal to century time scales due to the relatively long oceanic
514 residence time of Ba (≈10 kyr, Chan et al., 1976). Liu et al. (2019) have reported *Porites*
515 coral $\delta^{138/134}$Ba values ranging from 0.33 to 0.36‰ between 1987 and 1991 in the South
516 China Sea (YSR 9.6ºN/112.8ºE) (Fig. 1). Applying a $\Delta^{138/134}Ba_{coral\text{-}sw}$ value of -0.28 ‰
517 and the coral data in Eqn. (3), the estimated seawater $\delta^{138/134}$Ba values become +0.61 ~
518 +0.64 ‰, which agrees with the measured values (+0.60 ~ +0.64 ‰, A10
519 19.2ºN/115.5ºE and S504 19.7ºN/117.6ºE) in the water samples collected in 2010 (Cao
520 et al., 2020). These results suggest that the annual average $\delta^{138/134}$Ba values stay
521 constant over at least 20 years in the South China Sea surface water.

522 In contrast, the freshwater end-member $\delta^{138/134}$Ba and [Ba] values are likely to
523 be more variable. Bridgestock et al. (2021) have shown that Ba desorption from

suspended particles can significantly alter the estuarine [Ba] and $\delta^{138/134}$Ba compositions. To do a sensitivity test with different degrees of Ba desorption, we apply two freshwater effective end-members: (1) the Johor River ([Ba] = 1039 ± 319 nM, $\delta^{138/134}$Ba = 0.06 ± 0.12 ‰; Bridgestock et al., 2021) and (2) the regional average ([Ba] = 192 ± 30 nM, $\delta^{138/134}$Ba = 0.08 ± 0.03 ‰; Section 4.1) with the South China Sea values ($[Ba]_{sw}$ = 42 ± 1 nM, $\delta^{138/134}$Ba = 0.54 ± 0.02 ‰; Section 4.1) in the two end-members mixing model (Hsieh and Henderson, 2017). In Fig. 9, the mixing gradient of $\delta^{138/134}$Ba over salinity is not linear and flattens out when salinity is below 25 psu. Moreover, depending on the freshwater end-member Ba concentrations, the mixing trends between water $\delta^{138/134}$Ba values and salinity vary widely. For example, when $\delta^{138/134}$Ba value is at +0.1 ‰, the corresponding salinity can be anywhere between ~ 6 and ~ 24 psu.

Although the relationship between seawater $\delta^{138/134}$Ba and salinity values in the low salinity range (< 25 psu) is very sensitive to the freshwater end-member Ba concentrations, Singapore seawater $\delta^{138/134}$Ba and salinity data maintain a consistent relationship in the high salinity range (> 29 psu) over the sampling period (2012-2015), following the regional water mass mixing (Fig. 9b). This suggests that the regional freshwater end-member Ba compositions are relatively stable. Thus, Singapore seawater $\delta^{138/134}$Ba values can potentially be used as a tracer to reflect salinity changes within the range of this calibration (29 – 33 psu). Using the relationship established in Fig. 9b, the coral reconstructed seawater $\delta^{138/134}$Ba values can be converted into salinity (Fig. 10). The coral $\delta^{138/134}$Ba reconstructed seawater salinity follows the measured salinity seasonal cycle in the Singapore Strait. The results highlight the potential to extend the records to understand the dynamics of water mixing between the Malacca

548 Strait and the South China Sea, and hence the interaction with the Asian monsoon in
549 the past.

550 Through this work we have shown that shallow-water coral *Porites* can be used
551 as a reliable archive to record seawater $\delta^{138/134}$Ba values in the Singapore Strait, and the
552 potential of using it to trace salinity and water mass mixing in the past by demonstrating
553 the importance of calibrating the regional relationship between seawater $\delta^{138/134}$Ba and
554 salinity. The variation in freshwater end-member Ba compositions may hinder the use
555 of Ba isotopes as a paleo proxy for global seawater salinity. Nevertheless, if the regional
556 relationships between seawater $\delta^{138/134}$Ba values, water mass mixing and salinity can
557 be established, Ba isotopes can provide additional information about local and regional
558 water mixing and terrestrial runoffs in coastal oceans. A better constraint on the water
559 end-member Ba compositions could improve the use of Ba isotopes as paleo proxies in
560 shallow-water corals. Although every geochemical proxy or paleo-archive has its own
561 advantages and disadvantages, future studies with multiple tracers (e.g. $\delta^{138/134}$Ba, δ^{18}O
562 and Sr/Ca) and marine archives (e.g. corals and bivalve) from a wide range of
563 hydrological settings may provide more comprehensive detail to reconstruct the history
564 of freshwater runoff, water mass mixing, and climate and anthropogenetic activities in
565 coastal environments.

566

567 **5. Conclusions**

568 We present the first multi-colony Ba isotope calibration from three shallow-
569 water *Porites lutea* corals with the contemporaneous in-situ seawater data from the
570 Singapore Strait. Singapore waters show seasonal variations in Ba concentration and
571 isotope composition, which follow the seasonal salinity and monsoon-driven regional
572 water mass mixing between the Malacca Strait and the South China Sea and reflect the

strong influence of terrestrial inputs. The coral skeletal Ba/Ca and $\delta^{138/134}$Ba results in the three coral colonies generally follow the seasonal Ba variations in seawater. Despite the fact that the partition coefficient of Ba has a large uncertainty (D_{Ba} = 0.91 ± 0.29), the Ba isotope fractionation ($\Delta^{138/134}Ba_{coral\text{-}sw}$ = -0.28 ± 0.06 ‰) is relatively constant and shows no significant difference between these corals. The constant offset of Ba isotopes between coral skeletons and seawater allows the use of corals to record reliable seawater $\delta^{138/134}$Ba values in the past. The applications of Ba isotopes in coral skeletons can help to reconstruct the changes in Singapore Strait surface water salinity, and hence water mass mixing and the monsoon climate variability in the past.

Acknowledgments

We would like to thank Gonzalo Carrasco for sharing some of the water samples used in this study. We would also like to thank Phil Holdship for measuring water sample element compositions, and Jane Barling and Steve Wyatt for their assistance in the clean lab. We thank the editor and two anonymous reviewers for their constructive comments. The study was supported by the Royal Society Commonwealth Science Conference Fellow-on Grant (CSC\R1\170048) and the National Research Foundation Singapore (Marine Science Research and Development Programme project P03). We thank the National Park Board for allowing this research (NP/RP16-156-2a). We are grateful for the permissions to use the Malaysian water samples (Johor: P.T.N.J 3/8/6; Marine Park: JTLM 630-7 Jld. 4(17); Port Dickson: Prk.ML.S.04/32-2 Jld. 7(9)).

References

597 Allison, N., Cole, C., Hintz, C., Hintz, K., and Finch, A.A., 2018. Influences of coral
598 genotype and seawater pCO2 on skeletal Ba/Ca and Mg/Ca in cultured massive
599 Porites spp. corals. Palaeogeography, Palaeoclimatology, Palaeoecology 505, 351–
600 358.
601 Bates, S.L., Hendry, K.R., Pryer, H.V., Kinsley, C.K., Pyle, K.M., Woodward, E.M.S.,
602 and Horner, T.J., 2017. Barium isotopes reveal role of ocean circulation on barium
603 cycling in the Atlantic, Geochimica et Cosmochimica Acta 204, 286-299.
604 Bird, M.I., Pang, W.C., and Lambeck, K., 2006. The age and origin of the Straits of
605 Singapore. Palaeogeography, Palaeoclimatology, Palaeoecology 241, 531–538.
606 Brenner, L.D., Linsley, B.K., and Dunbar R.B., 2017. Examining the utility of coral
607 Ba/Ca as a proxy for river discharge and hydroclimate variability at Coiba Island,
608 Gulf of Chirqui, Panama. Marine Pollution Bulletin 118, 48–56.
609 Bridgetsock, L., Nathan, J., Paver, R., Hsieh, Y.-T., Porcelli, D., Tanzil, J., Holdship,
610 P., Carrasco, G., Vani Annammala, K., Swarzenski, P.W., and Henderson, G.M.,
611 2021. Estuarine processes modify the isotope composition of dissolved riverine
612 barium fluxes to the ocean. Chemical Geology, 579, 120340.
613 Cao, Z., Li., Y., Rao, X., Yu, Y., Hathorne, E.C., Siebert, C., Dai, M., Frank, M., 2020.
614 Constraining barium isotope fractionation in the upper water column of the South
615 China Sea. Geochimica et Cosmochimica Acta 288, 120–137.
616 Coffey, M., Dehairs, F., Collette, O., Luther, G., Church, T., and Jickells, T. 1997. The
617 behaviour of dissolved barium in estuaries. Estuarine, Coastal and Shelf Science 45,
618 113-121.
619 Crockford, P.W., Wing, B.A., Paytan, A., Hodgskiss, M.S.W., Mayfield, K.K., Hayles,
620 J.A., Middleton, J.E., Ahn, A-S.C., Johnson, D.T., Caxito, F., Uhlein, G., Halverson,

621 G.P., Eickmann, B., Torres, M., and Horner, T.J., 2019. Barium-isotopic constraints
622 on the origin of post-Marinoan barites, Earth and Planetary Science 519, 234-244.
623 Culkin, F. and Cox, R.A., 1966. Sodium, potassium, magnesium, calcium and strontium
624 in seawater. Deep Sea Research and Oceanographic Abstracts 13, 789–804.
625 Dietzel, M., Gussone, N., and Eisenhauer, A., 2004. Co-precipitation of Sr2+ and Ba2+
626 with aragonite by membrane diffusion of CO2 between 10 and 50 oC. Chemical
627 Geology 203, 139–151.
628 Evans, D., Gray, W.R., Rae, J.W.B., Greenop, R., Webb, P.B., Penkman, K., Kroger,
629 R., Allison, N., 2020. Trace and major element incorporation into amorphous
630 calcium carbonate (ACC) precipitated from seawater. Geochimica et Cosmochimica
631 Acta 290, 293-311.
632 Fallon, S.J., McCulloch, M.T., van Woesik, R., and Sinclair, D.J., 1999. Corals at their
633 latitudinal limits: laser ablation trace element systematics in Porites from Shirigai
634 Bay, Japan. Earth and Planetary Science Letter 172, 221–238.
635 Fleitmann, D., Dunbar, R.B., McCulloch, M., Mudelsee, M., Vuille, M., McClanahan,
636 T.R., Cole, J.E., and Eggins, S., 2007. East African soil erosion recorded in a 300
637 year old coral colony from Kenya. Geophysical Research Letter 34, L04401.
638 Gaetani, G.A., and Cohen, A.L., 2006. Element partitioning during precipitation of
639 aragonite from seawater: A framework for understanding paleoproxies. Geochimica
640 et Cosmochimica Acta 70, 4617–4634.
641 Geyman, B.M., Ptacek, J.L., LaVigne, M., and Horner, T.J., 2019. Barium in deep-sea
642 bamboo corals: Phase associations, barium stable isotopes & prospects for
643 paleoceanography. Earth and Planetary Science Letters 525, 115751.

644 Gonneea, M.E., Cohen, A.L., DeCarlo, T.M., and Charette, M.A., 2017. Relationship
645 between water and aragonite barium concentrations in aquaria reared juvenile corals.
646 Geochimica et Cosmochimica Acta 209, 123–134.
647 Hasan, G.M.J, van Maren, D.S., and Cheong, H.F., 2012. Improving hydrodynamic
648 modeling of an estuary in a mixed tidal regime by grid refining and aligning. Ocean
649 Dynamics 62, 395-409.
650 Hemsing, F., Hsieh, Y.-T., Bridgestock, L., Spooner, P.T., Robinson, L.F., Frank, N.,
651 and Henderson, G.M., 2018. Barium isotopes in cold-water corals. Earth and
652 Planetary Science Letters 491, 183–192.
653 Horner, T. J., Kinsley, C.W., and Nielsen, S.G., 2015. Barium-isotopic fractionation in
654 seawater mediated by barite cycling and oceanic circulation, Earth and Planetary
655 Science Letters 430, 511-522.
656 Horner, T.J., Pryer, H.V., Nielsen, S.G., Crockford, P.W., Gauglitz, J.M., Wing, B.A.,
657 and Ricketts, R.D., 2017. Pelagic barite precipitation at micromolar ambient sulfate.
658 Nature Communications, 8, 1242.
659 Hsieh, Y.T. and Henderson, G.M., 2017. Barium stable isotopes in the global ocean:
660 Tracer of Ba inputs and utilization. Earth and Planetary Science Letters 473, 269–
661 278.
662 Ito, S., Watanabe, T., Yano, M., Watanabe, T.K., 2020. Influence of local industrial
663 changes on reef coral calcification. Scientific Reports 10, 7892.
664 Joung, D. and Shiller, A.M., 2014. Dissolved barium behaviour in Louisiana Shelf
665 waters affected by the Mississippi/Atchafalaya River mixing zone. Geochimica et
666 Cosmochimica Acta 141, 303-313.

667 LaVigne, M., Grottoli, A.G., Palardy, J.E., and Sherrell, R.M., 2016. Multi-colony
668 calibrations of coral Ba/Ca with a contemporaneous in situ seawater barium record.
669 Geochimica et Cosmochimica Acta 179, 203–216.
670 Lea, D.W., Shen, G.T., and Boyle, E.A., 1989. Coralline barium records temporal
671 variability in equatorial Pacific upwelling. Nature 340, 373–376.
672 Lewis, S.E., Lough, J.M., Cantin, N.E., Matson, E.G., Kinsley, L., Bainbridge, Z.T.,
673 and Brodie, J.E., 2018. A critical evaluation of coral Ba/Ca, Mn/Ca and Y/Ca ratios
674 as indicators of terrestrial input: new data from the Great Barrier Reef, Australia.
675 Geochimica et Cosmochimica Acta 237, 131–154.
676 Liu, Y., Li, X., Zeng, Z., Yu, H.-M, Huang, F., Felis, T., and Shen, C.-C., 2019.
677 Annually-resolved coral skeletal d138/134Ba records: A new proxy for oceanic Ba
678 cycling. Geochimica et Cosmochimica Acta 247, 27–39.
679 Mass, T., Giuffre, A.J., Sun, C.-Y, Stifler, C.A., Frazier, M.J., Neder, M., Tamura, N.,
680 Stan, C.V., Marcus, M.A., and Gilbert, P.U.P.A., 2017. Amorphous calcium
681 carbonate particles from coral skeletons. Proceedings of the National Academy of
682 Sciences of the United States of America 114, E7670-E7678.
683 Mavromatis, V., van Zuilen, K., Purgstaller, B., Baldermann, A., Nagler, T.F., and
684 Dietzel, M., 2016. Barium isotope fraction- ation during witherite (BaCO3)
685 dissolution, precipitation and at equilibrium. Geochimica et Cosmochimica Acta
686 190, 72–84.
687 Mavromatis, V., Goetschl, K.E., Grengg, C., Konrad, F., Purgstaller, B. and Dietzel,
688 M., 2018. Barium partitioning in calcite and aragonite as a function of growth rate.
689 Geochimica et Cosmochimica Acta 237, 65–78.
690 Mavromatis, V., van Zuilen, K., Blanchard, M., van Zuilen, M., Dietzel, M., Schott, J.,
691 2020. Experimental and theoretical modelling of kinetic and equilibrium Ba isotope

692 fractionation during calcite and aragonite precipitation. Geochimica et
693 Cosmochimica Acta 269, 566–580.
694 McCulloch, M., Fallon, S., Wyndham, T., Hendy, E., Lough, J.M., and Barnes D., 2003.
695 Coral record of increased sediment flux to the inner Great Barrier Reef since
696 European settlement. Nature 421, 727–730.
697 Mollica, N.R., Guo, W., Cohen, A.L., Huang, K.-F., Foster, G.L., Donald, H.K., and
698 Solow, A.R., 2018. Ocean acidification affects coral growth by reducing skeletal
699 density. Proceedings of the National Academy of Sciences of the United States of
700 America 115, 1754-1759.
701 Montaggioni, L.F., Le Cornec, F., Correge, T., and Cabioch, G., 2006. Coral
702 barium/calcium record of mid-Holocene upwelling activity in New Caledonia,
703 South-West Pacific. Palaeogeography, Palaeoclimatology, Palaeoecology 237, 436–
704 455.
705 Nagtegaal, R., Grove, C.A., Kasper, S., Zinke, J., Boer, W.G., and Brummer, J.A.,
706 2012. Spectral luminescence and geochemistry of coral aragonite: effects of whole-
707 core treatment. Chemical Geology 318–319, 6–15.
708 Pretet, C., van Zuilen, K., Nägler, T.F., Reynaud, S., Böttcher, M.E., Samankassou, E.,
709 2016. Constraints on barium isotope fractionation during aragonite precipitation by
710 corals. The Depositional Record 1, 118–129.
711 Reuer, M.K., Boyle, E.A., and Cole, J.E., 2003. A mid-twentieth century reduction in
712 tropical upwelling inferred from coralline trace element proxies. Earth and Planetary
713 Science Letters 210, 437–452.
714 Saha, N., Webb, G.E., and Zhao, J.-X., 2016. Coral skeletal geochemistry as a monitor
715 of inshore water quality. Science of The Total Environment 566–567, 652–684.

716 Shen, G.T. and Boyle, E.A., 1988. Determination of lead, cadmium and other trace
717 metals in annually-banded corals. Chemical Geology 67, 47–62.
718 Sinclair, D.J., 2005. Non-river flood barium signals in the skeletons of corals from
719 coastal Queensland, Australia. Earth and Planetary Science Letters 237, 354–369.
720 Stewart, J.A., Christopher, S.J., Kucklick, J.R., Bordier, L., Chalk, T.B., Dapoigny, A.,
721 Douville, E., Foster, G.L., Gray, W.R., Greenop, R., Gutjahr, M., Hemsing, F.,
722 Henehan, M.J., Holdship, P., Hsieh, Y.-T., Kolevica, A., Lin, Y.-P., Mawbey, E.M.,
723 Rae, J.W.B., Robinson, L.F., Shuttleworth, R., You, C.-F., Zhang, S., Day, R.D.,
724 2020. NIST RM 8301 boron isotopes in marine carbonate (simulated coral and
725 foraminifera solutions): inter-laboratory d11Ba and trace element ratio value
726 assignment. Geostandards and Geoanalytical Research, doi.org/10.1111.ggr.12363.
727 Swart, P.K., Healy, G., Greer, L., Lutz, M., Saied, A., Anderegg, D., Dodge, R.E. and
728 Rudnick, D., 1999. The use of proxy chemical records in coral skeletons to ascertain
729 past environmental conditions in Florida Bay. Estuaries 22, 384-397.
730 Tanzil, J.T.I., Lee, J.N., Brown, B.E., Quax, R., Kaandorp, J.A., Lough, J.M., and Todd,
731 P.A., 2016. Luminescence and density banding patterns in massive Porites corals
732 around the Thai- Malay Peninsula, Southeast Asia. Limnology and Oceanography
733 61, 2003–2026.
734 Tanzil, J.T.I., Goodkin, N.F., Sin, T.M., Chen, M.L., Fabbro, G.N., Boyle, E.A., Lee,
735 A.C., and Toh, K.B., 2019. Multi-colony coral skeletal Ba/Ca from singapore's
736 turbid urban reefs: Relationship with contemporaneous in-situ seawater parameters.
737 Geochimica et Cosmochimica Acta 250, 191–208.
738 Taylor, J.R., Falkner, K.K., Schauer, U., and Meredith, M., 2003. Quantitative
739 considerations of dissolved barium as a tracer in the Arctic Ocean. Journal of
740 Geophysical Research 108, 3374.

741 Tudhope, A.W., Lea, D.W., Shimmield, G.B., Chilchott, C.P., and Head, S., 1996.
742 Monsoon climate and Arabian Sea coastal upwelling recorded in massive corals
743 from Southern Oman. PALAIOS 11, 347–361.
744 Van Maren, D.S. and Gerritsen, H., 2012. Residual flow and tidal asymmetry in the
745 Singapore Strait, with implications for resuspension and residual transport of
746 sediment. Journal of Geophysical Research 117, C04021.
747 Walther, B.D., Kingsford, M.J., and McCulloch, M.T., 2013. Environmental records
748 from Great Barrier Reef corals: inshore versus offshore drivers. PLoS One 8,
749 e77091.
750 Yamazaki, A., Yano, M., Harii, S., and Watanabe, T., 2021. Effect of light on the Ba/Ca
751 ratios in coral skeletons. Chemical Geology 559, 119911.
752 Zweng, M.M., Reagan, J.R., Seidov, D., Boyer, T.P., Locarnini, R.A., Garcia, H.E.,
753 Mishonov, A.V., Baranova, O.K., Weathers, K., Paver, C.R., and Smolyar, I.,
754 2018. World Ocean Atlas 2018, Volume 2: Salinity. Mishonov, A., Technical
755 Editor, NOAA Atlas NESDIS 82, 50 pp.
756
757
758
759
760
761
762
763
764
765

Figures

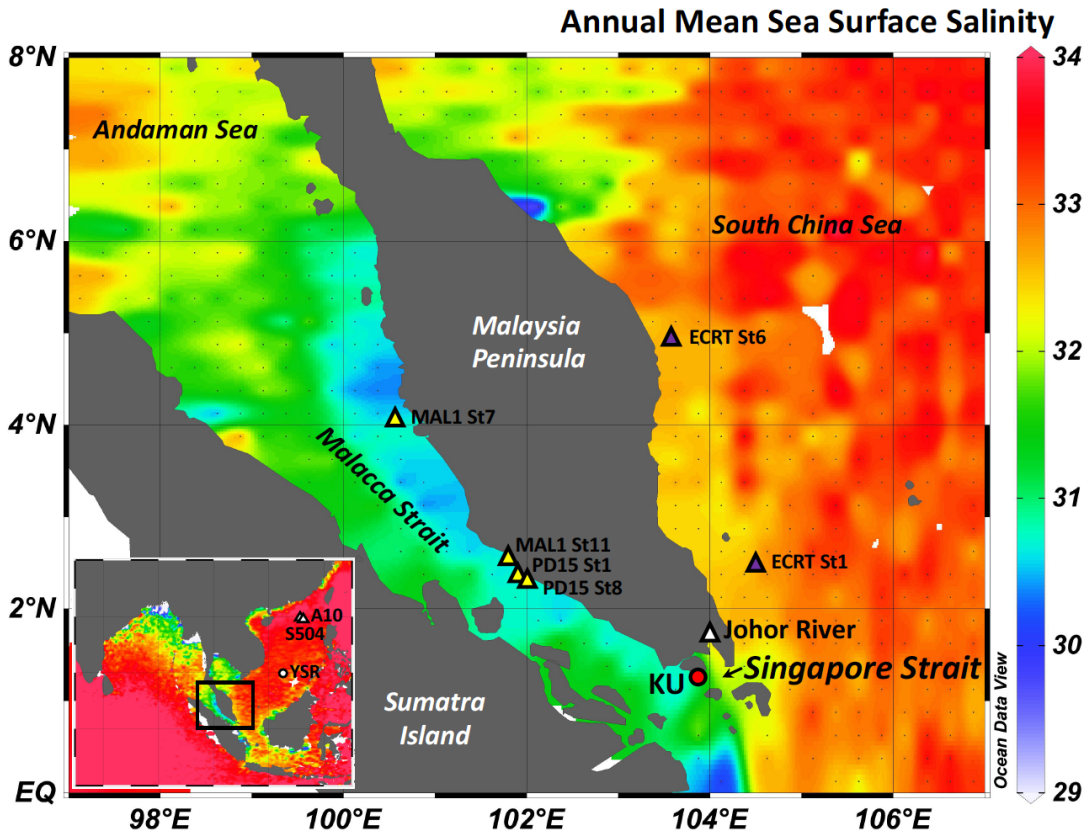

Figure 1 Map of sampling locations and the distribution of annual mean sea surface salinity. The sample locations from previous studies are labeled for references: the South China Sea water (A10 and S504, Cao et al., 2020) and coral samples (YSR, Liu et al., 2019) and the Johor River estuary (Bridgestock et al., 2021). The annual mean sea surface salinity data are from the World Ocean Atlas 2018 (Zweng et al., 2018).

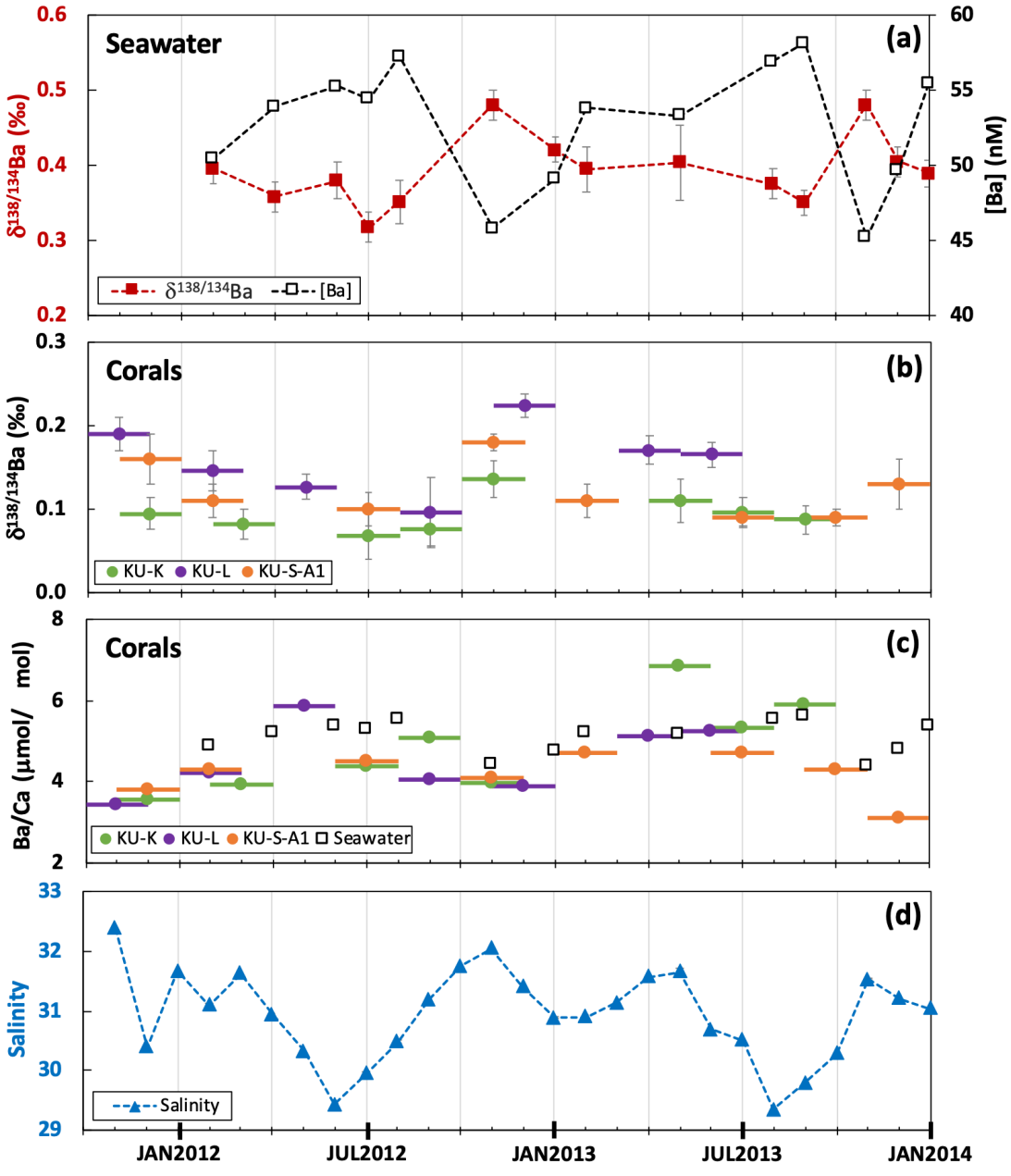

Figure 2 Time-series data of **(a)** seawater Ba concentrations isotope compositions, (b) coral skeletal Ba isotope compositions, (c) coral skeletal and seawater Ba/Ca ratios, and (d) in-situ surface seawater salinity data from November 2011 to January 2014 in the KU site in the Singapore Strait. The data from three coral colonies are labeled in green (KU-K), purple (KU-L) and orange (KU-S-A1). The error bars for the Ba data represent 2 standard deviations (± 2SD), and are within the size of the symbols for [Ba] and

788 Ba/Ca. The coral skeletal Ba data are labeled with a 3-month time span (± 1 month) to
789 reflect the sample resolution.
790

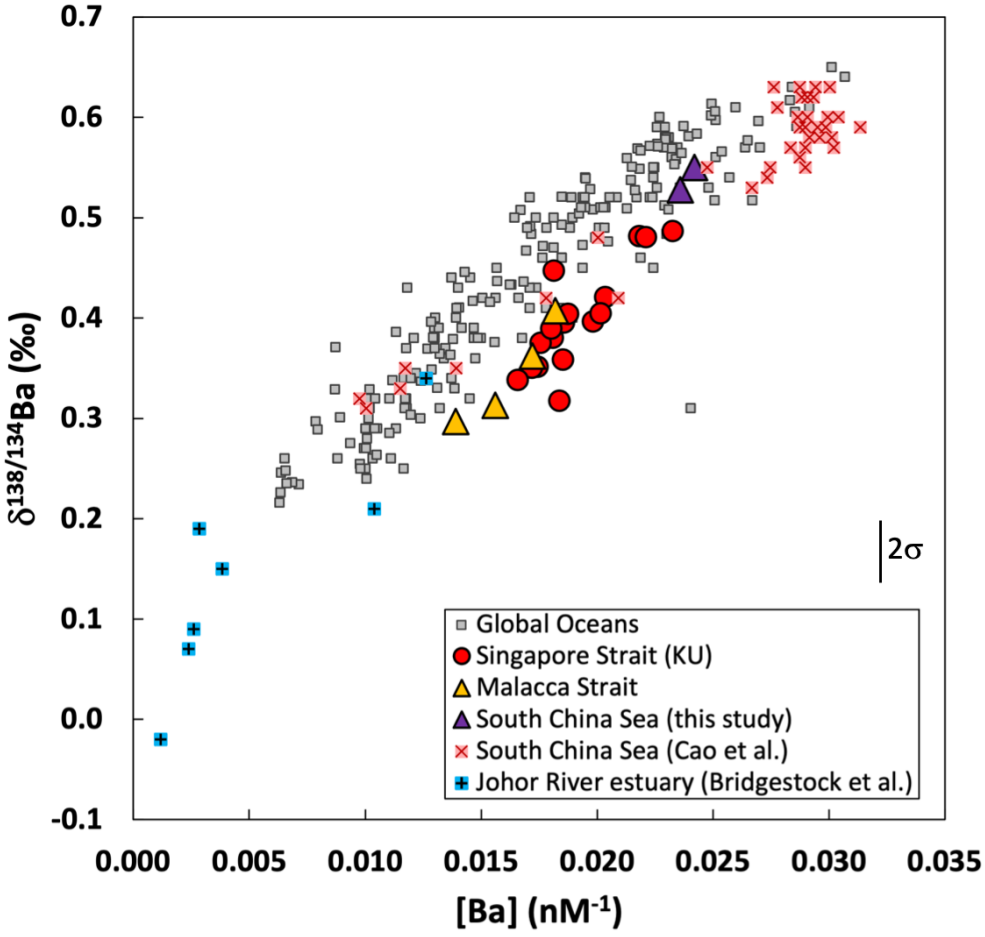

791

792 **Figure 3** Ba isotope compositions versus 1/[Ba] for all water samples from this study,
793 the Johor River estuary (Bridgestock et al., 2021), the South China Sea (Cao et al.,
794 2020) and the global oceans (Horner et al., 2015; Bates et al., 2017; Hsieh and
795 Henderson, 2017; Bridgestock et al., 2018; Hemsing et al., 2018; Geyman et al., 2019).
796 The error bar (±2σ) of $\delta^{138/134}$Ba from this study is shown.
797

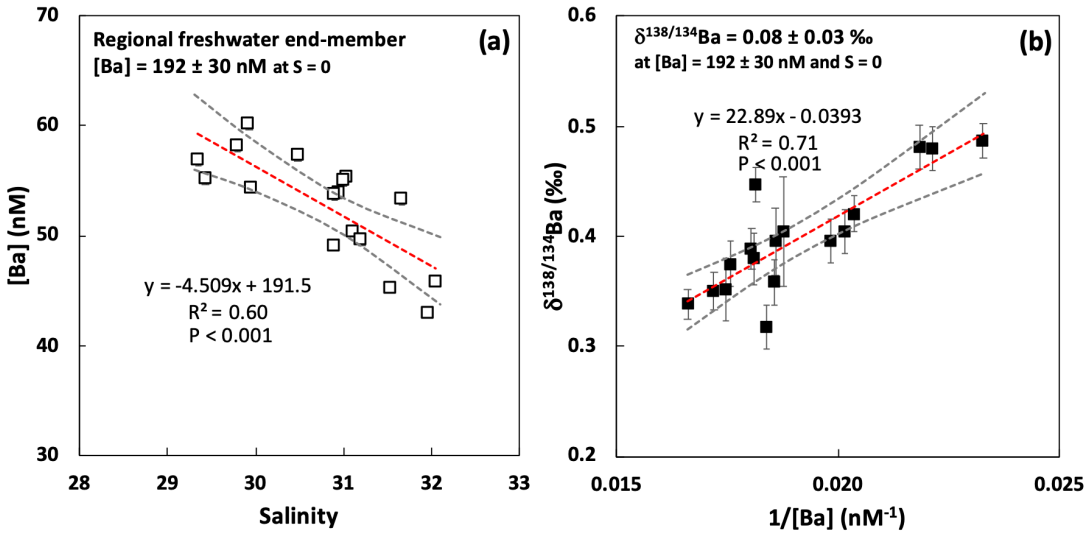

798

799 **Figure 4** Relationships between (a) seawater Ba concentration and salinity, and (b)
800 seawater Ba isotope composition and 1/Ba concentration in the Singapore Strait. The
801 red dashed lines denote linear regression with 95% confidence intervals in the grey
802 dashed lines. The linear regressions are used to extrapolate the effective regional
803 freshwater end-member [Ba] and $\delta^{138/134}$Ba compositions at salinity zero.

804

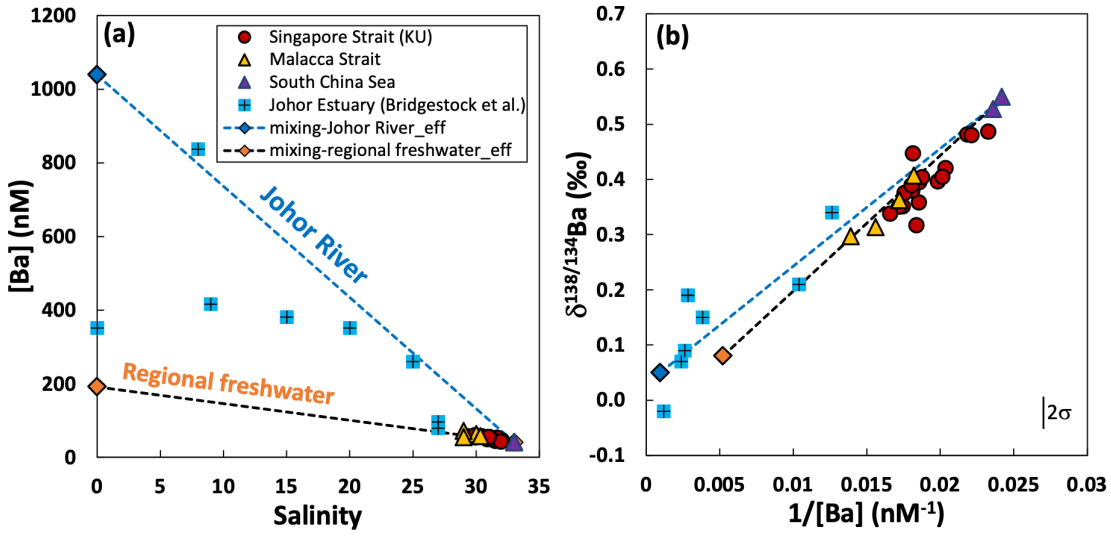

805

806 **Figure 5** Relationships between (a) water Ba concentration and salinity, and (b) water
807 Ba isotope composition and 1/Ba concentration in the Singapore seawater and the
808 regional water masses. The dashed lines denote the mixing lines between the average
809 of the South China Sea water (purple tringles) and two effective riverine end-members

(the Johor River: blue diamonds, Bridgestock et al., 2021; the regional freshwater average: orange diamond, this study). The Malacca Strat data (yellow tringles) and the Singapore Strait data (red circles) generally lie on the mixing line between the South China Sea and the regional freshwater end-members. The error bar (±2σ) of $\delta^{138/134}$Ba from this study is shown.

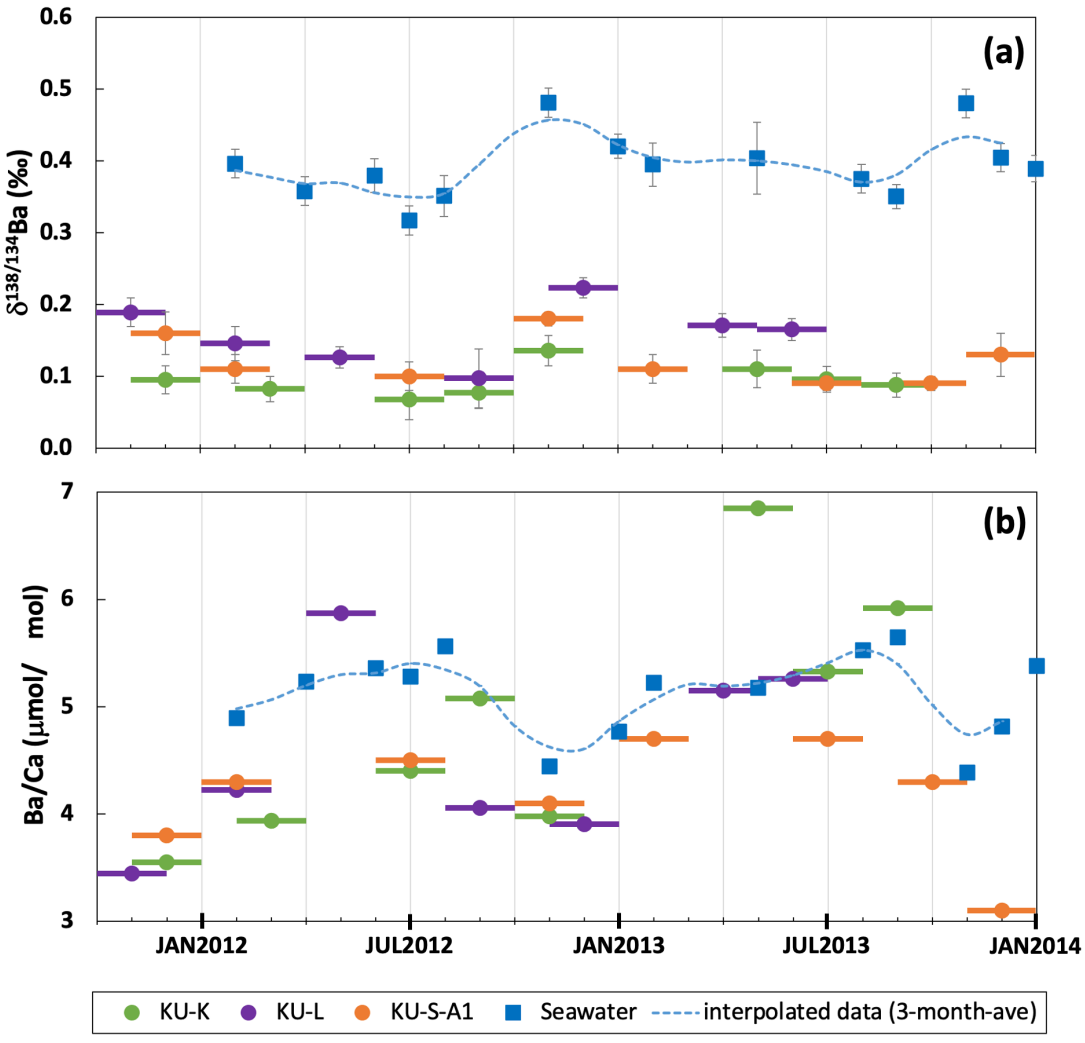

Figure 6 Coral skeletal (a) Ba isotope compositions and (b) Ba/Ca ratios from November 2011 to January 2014 in the three coral colonies (KU-K, KU-L and KU-S-A1) in the Singapore Strait. The KU water Ba isotope and concentration data are shown for comparison. To match the coral and water sample resolutions, the dashed lines are

taken from the 3-month average values, based on both the interpolated and measured data (Table S3).

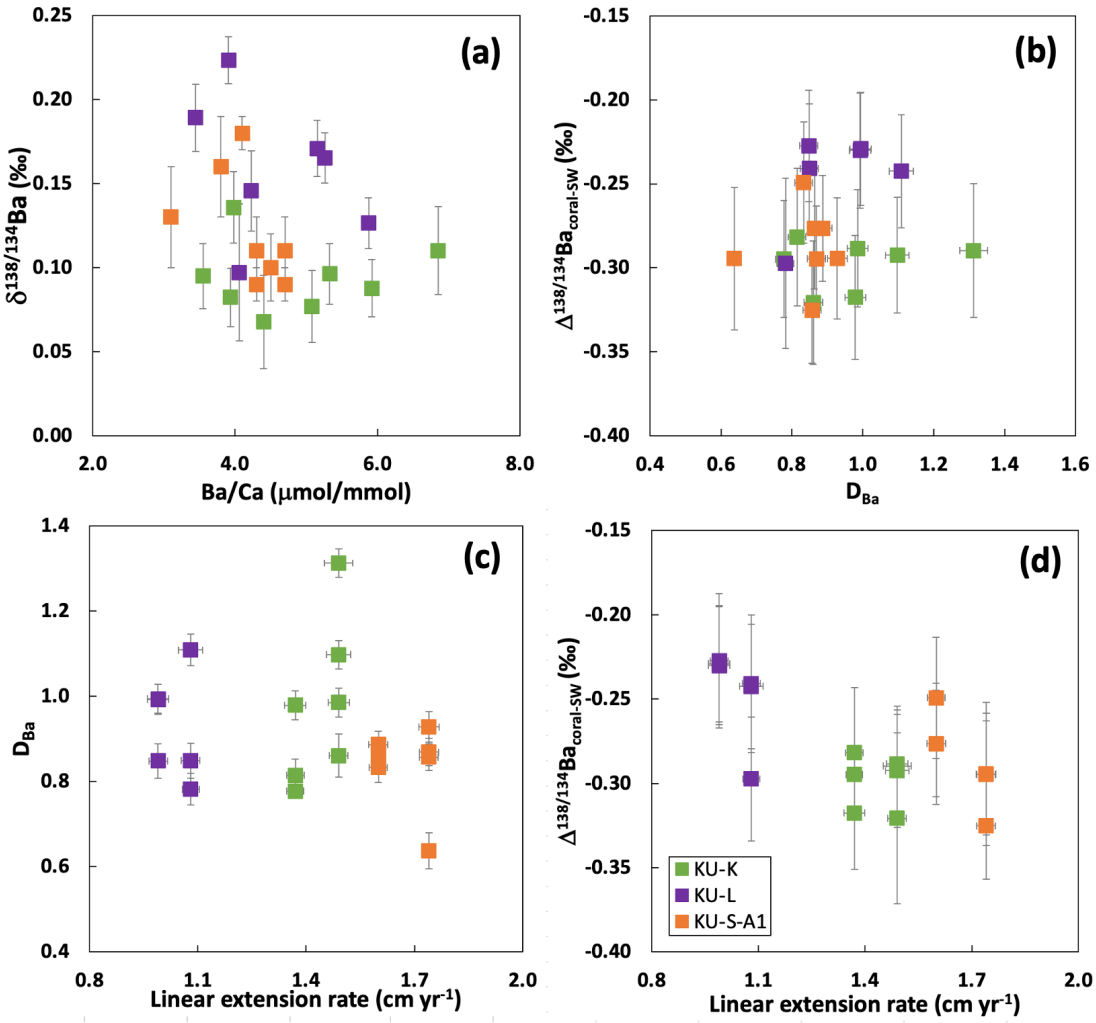

Figure 7 Relationships between coral skeletal (a) $\delta^{138/134}$Ba and Ba/Ca; (b) Ba isotope fractionation factor ($\Delta^{138/134}Ba_{coral\text{-}sw}$) and partition coefficient (D_{Ba}); (c) D_{Ba} and the linear extension rates; and (d) $\Delta^{138/134}Ba_{coral\text{-}sw}$ and the linear extension rates. The error bars represent 2 standard deviations (± 2σ).

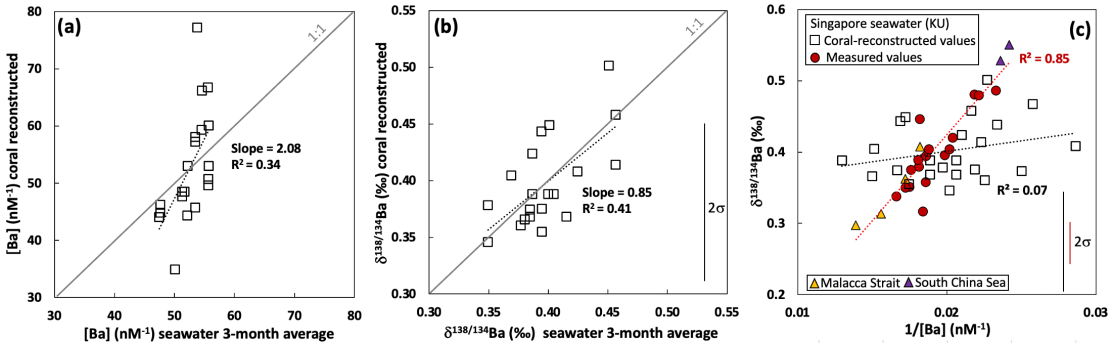

Figure 8 Relationships between the coral reconstructed and the measured seawater (a) [Ba] and (b) $\delta^{138/134}$Ba values. In (a) and (b), the measured seawater values are based on the 3-month average data (Table S3). The 1:1 and linear regression slopes are provided for comparison. (c) The relationship between seawater $\delta^{138/134}$Ba and 1/[Ba] in the measured (solid red circles) and the coral reconstructed water values from the KU corals (open squares). The dashed lines denote the linear regression through the coral reconstructed water values (black) and the measured water data including the regional water masses (red). The error bars (2σ) of $\delta^{138/134}$Ba are shown in black (coral) and red (water).

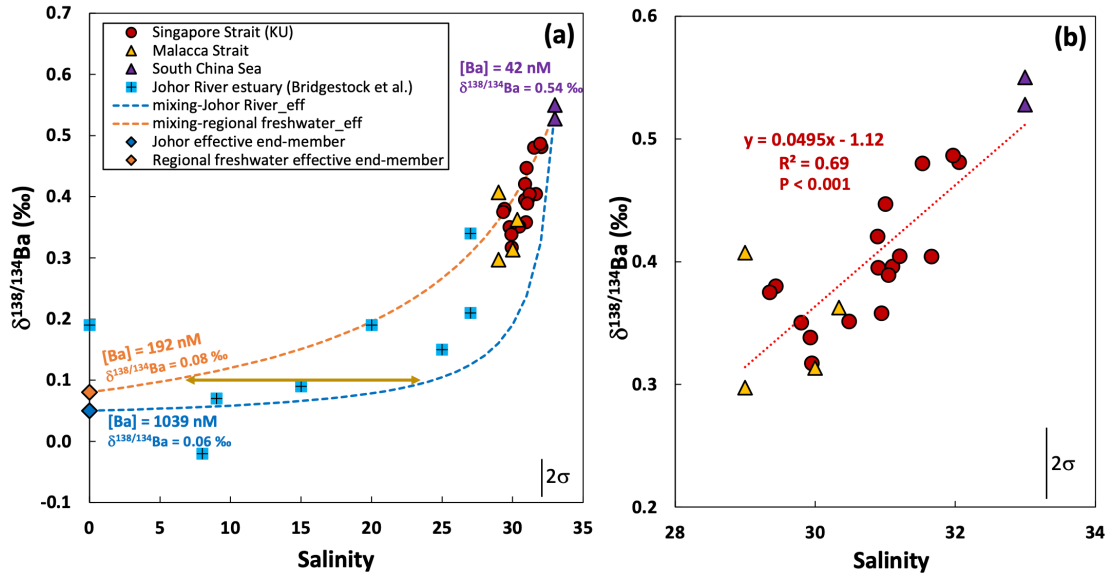

Figure 9 Water Ba isotope composition and salinity mixing relationships between the South China Sea and freshwater waters in the Singapore Strait. (a) The dashed lines

represent the end-member mixing trends between the average of the South China Sea water (purple tringles) and two effective freshwater end-member values (the Johor River: blue diamond, Bridgestock et al., 2021; the regional freshwater: orange diamond, this study). The horizonal brown line indicates a range of possible salinity values corresponding to a water $\delta^{138/134}$Ba value at 0.1 ‰. (b) The relationship between seawater $\delta^{138/134}$Ba values and salinity in the Singapore Strait (KU) and the regional waters. The dashed red line denotes the linear regression through the data, including the regional waters. The error bars (2σ) of $\delta^{138/134}$Ba are shown.

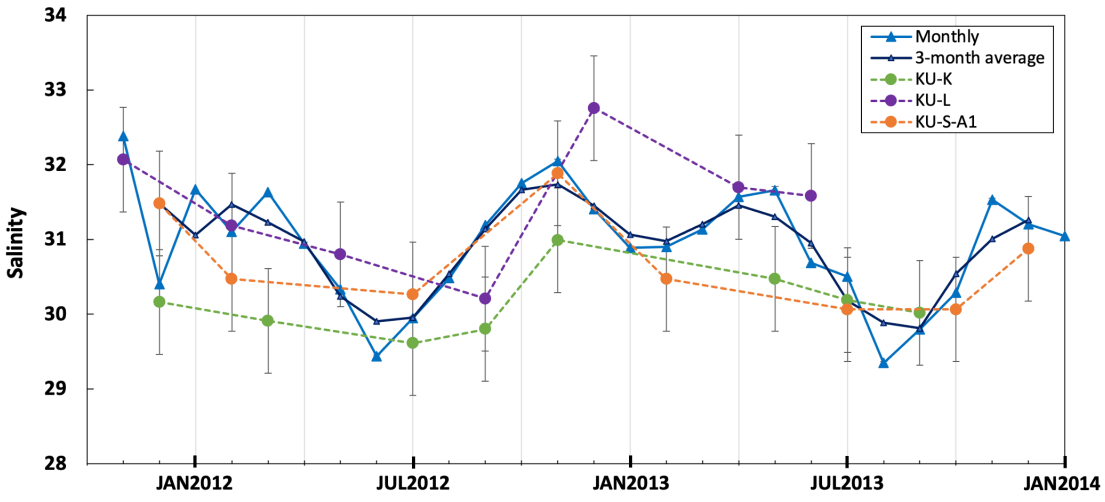

Figure 10 Comparison between the coral $\delta^{138/134}$Ba reconstructed seawater salinity and in-situ measured salinity data (monthly and 3-month average) between November 2011 and January 2014 in the KU site in the Singapore Strait. The error bars for the coral constructed salinity (± 0.7 psu, 1σ) represent the uncertainties of coral and seawater calibrations.